JOURNAL OF THE ROYAL SOCIETY Interface

J. R. Soc. Interface (2006) **3**, 805–821
doi:10.1098/rsif.2006.0144
Published online 8 August 2006

Bioactive and bioresorbable cellular cubic-composite scaffolds for use in bone reconstruction

Yasuo Shikinami[1,*], Kenshi Okazaki[1], Makoto Saito[1], Masaki Okuno[1], Shin Hasegawa[2], Jiro Tamura[2], Shunsuke Fujibayashi[2] and Takashi Nakamura[2]

[1]*Medical Division, Takiron Co., Ltd, 2-3-13, Azuchi-machi, Chuo-ku, Osaka 541-0052, Japan*
[2]*Department of Orthopaedic Surgery, Graduate School of Medicine, Kyoto University, 54 Kawahara-cho, Shogoin, Sakyo-ku, Kyoto 606-8507, Japan*

We used a novel composite fibre-precipitation method to create bioactive and bioresorbable cellular cubic composites containing calcium phosphate (CaP) particles (unsintered and uncalcined hydroxyapatite (u-HA), α-tricalcium phosphate, β-tricalcium phosphate, tetracalcium phosphate, dicalcium phosphate dihydrate, dicalcium phosphate anhydrate or octacalcium phosphate) in a poly-D/L-lactide matrix. The CaP particles occupied greater than or equal to 70 wt% (greater than or equal to 50 vol%) fractions within the composites. The porosities of the cellular cubic composites were greater than or equal to 70% and interconnective pores accounted for greater than or equal to 70% of these values. *In vitro* changes in the cellular geometries and physical properties of the composites were evaluated over time. The Alamar Blue assay was used to measure osteoblast proliferation, while the alkaline phosphatase assay was used to measure osteoblast differentiation. Cellular cubic C-u-HA70, which contained 70 wt% u-HA particles in a 30 wt% poly-D/L-lactide matrix, showed the greatest three-dimensional cell affinity among the materials tested. This composite had similar compressive strength and cellular geometry to cancellous bone, could be modified intraoperatively (by trimming or heating) and was able to form cortico-cancellous bone-like hybrids. The osteoinductivity of C-u-HA70, independent of biological growth factors, was confirmed by implantation into the back muscles of beagles. Our results demonstrated that C-u-HA70 has the potential as a cell scaffold or temporary hard-tissue substitute for clinical use in bone reconstruction.

Keywords: bioactive; bioresorbable; bone substitutes; cell scaffolds; composites

1. INTRODUCTION

The current study evaluated the potential clinical uses of novel cellular cubic-composite materials as cell scaffolds and temporary bone substitutes in the hard-tissue reconstruction of large defects, such as those produced by surgical debridement in tumoural, traumatic, osteolytic and infectious regions. Cell scaffolds for use in hard-tissue-engineering applications should have the following properties: biological safety, three-dimensional cell affinity (i.e. the capacity for seeded cells to be evenly and extensively distributed across their surface), bioactivity including osteoconduction (i.e. the potential for ossification to occur in the region of existing bone tissues) and osteoinduction (i.e. the potential for ossification to occur in a region where bone tissues are absent), adequate strength, which lasts until complete tissue regeneration has been realized; timely bioresorption during tissue replacement and eventual total replacement accompanied by restoration of the natural shape of the defective tissue. In addition, surgeons require these devices to be easy to handle and to have the ability to be modified intraoperatively (for example, by trimming or heating).

A great number of porous cell scaffolds have previously been developed for tissue-engineering applications in bone or cartilage reconstruction (Slivka *et al.* 2001; Yang *et al.* 2001). Most consisted of separate bioceramics or bioresorbable polymers, with the exception of a few promising composites that have included both (Roy *et al.* 2003; Rezwan *et al.* 2006). These materials have tended to lack practical utility.

Cellular bioceramic-only scaffolds comprised of hydroxyapatite (HA)—the main source of the calcium phosphate (CaP) found in natural bone—or β-tricalcium phosphate (β-TCP) have high porosity and are fragile, slowly absorbed and not readily replaced with natural bone tissues. We have to carefully choose CaP

*Author for correspondence (sikinami@takiron.co.jp).

Received 26 May 2006
Accepted 5 July 2006

Table 1. Physicochemical properties of CaP particles.

CaP particles	chemical formula	Ca/P	pH[a]	density (g cm^{-3})	crystal form[b]
u-HA	$Ca_{10}(PO_4)_6(OH)_2$	1.67	6.90	2.70	hexagonal columnar
α-TCP	$Ca_3(PO_4)_2$	1.50	8.72	2.87	spheroid
β-TCP	$Ca_3(PO_4)_2$	1.50	9.41	3.07	spheroid
TeCP	$Ca_4(PO_4)_2{\cdot}O$	2.00	11.60	3.37	spheroid
DCPA	$CaHPO_4$	1.00	6.88	2.37	lamellar
DCPD	$CaHPO_4{\cdot}2H_2O$	1.00	6.53	2.92	lamellar
OCP	$Ca_8H_2(PO_4)_6{\cdot}5H_2O$	1.33	6.64	2.67	lamellar

[a] pH values of particulate bioceramics in 10% aqueous solution were measured using a pH metre at 25 °C.
[b] Any CaP particle that formed secondary aggregations was grounded into particles (average size 3–5 μm) using a wet batch-type grinder (BSG-1/4G; Aimex Co., Ltd).

particles with satisfactory bioresorbability, which actually fit for a use.

By contrast, cellular bioresorbable polymer-only scaffolds are flexural, have low-rigidity and are elastic substances. These materials have inadequate three-dimensional cell affinities, osteological bioactivities and degradation rates. Examples include poly-glycolic acid (PGA) and poly-L-lactide (PLLA), which degrade too quickly and too slowly, respectively, for use in cell scaffolds and have poor cell affinity (Wan *et al.* 2006).

We therefore used an original composite fibre-precipitation (CFP) method to produce novel cellular cubic composites of both types of material, in order to meet the essential requirements described above. These composites comprised one of the seven types of bioresorbable and bioactive CaP particle (i.e. unsintered and uncalcined hydroxyapatite (u-HA), α-TCP, β-TCP, tetracalcium phosphate (TeCP), dicalcium phosphate dihydrate (DCPD), dicalcium phosphate anhydrate (DCPA) or octacalcium phosphate (OCP)) within a bioresorbable poly-D/L-lactide (P(D/L)LA) or poly-glycolic acid/DL-lactide (PGA/(D/L)LA) polymer matrix. CaP particles with an average size of 3–5 μm were used, as they produced porous composites with bioactivities and moderate rates of resorption. These particles occupied greater than or equal to 70 wt% (greater than or equal to 50 vol%) fractions of the cellular cubic composites. In addition, the composites had porosities of greater than or equal to 70%, and interconnective pores accounted for greater than or equal to 70% of the total values. These specifications, especially in the case of the cellular cubic u-HA/P(D/L)LA composite, conferred to the following favourable characteristics: similar compressive strength (Sc) to natural cancellous bone; optimal bioactivity; good three-dimensional cell affinity and adequate plasticity of the polymer matrix to allow it to be modified intraoperatively.

We initially identified the bioresorbable polymer (P(D/L)LA) that performed best in combination with bioactive and bioresorbable CaP particles. This was achieved by evaluating cell proliferation and differentiation through the *ex vivo* two-dimensional culturing of normal human osteoblasts (HOBs) on each composite sheet. We then determined the most suitable CaP particles for inclusion in cellular cubic composites by evaluating the porosity, pore size, pore geometry and pore interconnection and mechanical strength. Our findings suggested that cellular cubic u-HA70 (C-u-HA70), containing 70 wt% u-HA particles in 30 wt% P(D/L)LA, represented the optimal combination. We then evaluated several characteristics of C-u-HA70, including the *in vitro* time-dependent changes in Sc, the viscosity average molecular weight ($\overline{Mv}$) and the interconnective pore geometry, as well as the rates of cell proliferation and differentiation through *ex vivo* three-dimensional culturing of HOBs. We also examined the potential for osteoinduction by implanting C-u-HA70 into the back muscles of beagles.

In addition, we examined the potential for modifying C-u-HA70 intraoperatively by trimming or thermal transform to adjust it to the shape of a defect. Moreover, we evaluated its ability to produce cortico-cancellous hybrids in combination with artificial cortical bone-like composites, which have total resorbability, a favourable degradation rate and mechanical strengths comparable to those of normal bone (Shikinami & Okuno 1999).

The current report demonstrates the suitability of C-u-HA70 for use as a cell scaffold or temporary bone substitute and confirms its potential clinical application in hard-tissue reconstruction.

2. MATERIAL AND METHODS

The physicochemical properties of the seven types of CaP particle investigated are listed in table 1.

2.1. Preparation of non-porous sheet composites

Sheet composites (∅14×0.7 mm), containing a homogeneous mixture of each respective CaP particle in a P(D/L)LA ($\overline{Mv}$; 77 kDa) matrix, were prepared by the hot-compression moulding of non-woven composite fibres. The fibres were produced by spraying with a homogeneous mixture of CaP particles and P(D/L)LA. All the composites contained 70 wt% of the respective CaP particle, with the exception of the OCP/P(D/L)LA sheet, which contained 50 wt% OCP particles because the 70 wt% material was too fragile. A P(D/L)LA-only sheet was produced by the same method and used as a control.

2.2. Preparation and evaluation of cellular cubic composites (three-dimensional interconnective porous composites)

Cellular cubic composites containing a homogeneous 70 wt% fraction of the relevant CaP particle in a P(D/L)LA or PGA/(D/L)LA matrix, each of which had an $\overline{\text{Mv}}$ value of 77 kDa, were fabricated using the composite fibre-precipitation (CFP) method (Shikinami 2003). Non-woven fibres, which were produced by spraying a homogeneous mixture of CaP particles/P(D/L)LA or PGA/(D/L)LA, were fused into a cellular cubic composite. This was achieved by inducing the fibres to swell within a volatile solvent while located inside an airtight chamber that was undergoing decompression. Samples with porosities ranging from 50 to 90% were prepared for each combination of materials; however, all of the porous substances were too fragile to be handled at a 90 : 10 weight ratio. For u-HA/P(D/L)LA, the fraction of u-HA particles was successfully varied from 50 to 80 wt% in order to examine the accompanying changes in mechanical strength. The pore sizes and distribution changes over time were calculated from micro-computed tomography (μCT) images produced by a Desktop Micro CT 1072 (SkyScan; 103 kV and 102 μA) and mercury-intrusion porosimetry (Micro Meritics Autopore IV 9520 type; Shimazu Co., Ltd). The continuous porosity was calculated by measuring the difference between the weights of sample blocks that were fully immersed in ethanol solution and those that were completely dried in air.

2.3. Changes in mechanical strength in vitro

The degradation behaviours of the composites over time were tested under *in vitro* conditions. Each substance was immersed in simulated body fluid (SBF) at 37 °C. Changes in $\overline{\text{Mv}}$ and Sc were measured using the standard methods (Shikinami & Okuno 1999). The Sc of each cylindrical sample (∅6.0×15 mm) was measured in air using a Shimadzu AGS-200D Autograph tester according to standard 604 of the International Standards Organisation (ISO 604) and was calculated using the following equation:

$$\text{Sc(MPa)} = \frac{F_{\max}}{A}.$$

Here, $F_{\max}$ is the maximum force (N) and A is the compressive area (mm^2).

The $\overline{\text{Mv}}$ of the P(D/L)LA alone, after the CaP particles had been filtered off from a composite/chloroform solution, was calculated based on the Mark-Houwiks formula (Schindler & Harper 1979), by measuring the intrinsic viscosity $[\eta]$ at 30 °C using an Ostwald viscometer and substituting the value into the equation

$$[\eta] = 2.12 \times 10^{-4} \overline{\text{Mv}}^{0.77}.$$

In vitro changes in Sc and $\overline{\text{Mv}}$ were measured over the specific time periods shown in table 2. For all parameters, three samples were measured and the mean values and the standard deviations were calculated.

Table 2. Immersion period for *in vitro* changes.

	immersion period (weeks)
Sc	4, 8, 12, 24, 36, 52
$\overline{\text{Mv}}$	
C-u-HA70	1, 2, 4, 6, 8, 10, 12, 16, 20, 24, 30, 36, 42, 52, 78
C-β-TCP70	2, 4, 6, 8, 12, 16, 20, 24, 30, 36, 42, 52, 78
C-OCP50	1, 2, 4, 6, 8, 12, 16, 24, 36, 52, 78

2.4. Changes in structural porosity in vitro

The internal structural porosity was observed using scanning electron microscopy (SEM) with a Hitachi S-2460N. *In vitro* changes in structural porosity over time were studied using μCT images.

2.5. Other properties

Ideally, cell scaffolds should have the ability to be manipulated intraoperatively in order to adjust to the shape of a defect. This ability can ultimately determine the success of reconstructive surgery. We therefore tested the potential for the composites to be trimmed with operating scissors or transformed by heating at a temperature slightly above the glass-transition temperature (T_g) of 65 °C.

2.5.1. Transformation and insertion procedures. A C-u-HA70 cylinder (∅18×H 18 mm; Comporus) was immersed in physiological saline at 65 °C. The softened column was adjusted by hand to match the dimensions of a sample, a rectangular-shaped defect (18 mm major axis ×16 mm minor axis) that had been introduced into a tibial saw bone. The cylinder was inserted into the bone after it had been allowed to cool naturally.

2.5.2. Trimming procedures. A square C-u-HA70 plate was trimmed into a round sheet using operating scissors. The edges of a C-u-HA70 block were removed by shaving with a scalpel.

2.6. Osteoblast affinities in cell cultures

All the samples used in the cell cultures and the animal experiments detailed below were sterilized with 20 wt% ethylene oxide gas (EOG) and 80 wt% CO_2 at 45 °C for 5 h with 50% H_2O. The remaining gas was removed by aeration at 45 °C and any residual volatile solvent from the production process was removed by evacuation until it was no longer detectable by gas chromatography.

The two- and three-dimensional osteoblast-cell affinities were examined as follows (Lohmann *et al.* 2002). Initially, non-porous sheets (∅14×0.7 mm) of six different types (S-u-HA70, S-β-TCP70, S-OCP50, S-α-TCP70, S-DCPD70 and S-TeCP70) were examined to validate the two-dimensional cell affinity. A P(D/L)LA-only sheet was used as a control. Based on the findings, cellular cylindrical blocks (∅13×2.0 mm) of the following four types were used as carriers in

three-dimensional cultures of HOBs (Clonetics; Lot No. 2F1968): C-u-HA70, C-β-TCP70, C-DCPD70 and C-TeCP70, Cellular P(D/L)LA alone, and s-HA(C-s-HA) (CELLYARD; Pentax Corp.) with a porosity of approximately 50% and a pore size of 5–100 μm, were used as controls. The C-s-HA was examined after 10 days, at which time the three-dimensional cell cultures should have been saturated. For all of the experiments, the cells were cultured using osteoblast growth medium (OGM; Clonetics), in a humidified incubator with 5% CO_2 at 37 °C. The growth medium comprised osteoblast basal medium supplemented with 10% foetal bovine serum (FBS), 20–30 mg l^{-1} ascorbic acid, 50 mg l^{-1} gentamicin and 50 μg l^{-1} amphotericin B. The cells were received in cryovials and were passaged twice before use. The osteoblasts were suspended in OGM solution at concentrations of 5.0×10^4 and 1.0×10^5 cells ml^{-1} for the sheet composites and the cellular cubic composites, respectively. The indicated doses within a 1 ml suspension were seeded onto each sheet or cellular cubic-composite in a 24-well plate and cultured in a humidified incubator for 24 h. The sheet or cellular cubic-composite was then placed in a six-well plate and cultured in 5 ml OGM for 9 days. The culture medium was replaced every 3 days.

Three specimens were tested for each condition and the average values were calculated. Three specimens were deemed to be sufficient as both the cell-proliferation rates and the differentiation rates were examined simultaneously.

2.7. Analysis of cell response

The Alamar Blue assay (Ahmed *et al.* 1994) and the alkaline phosphatase (ALP) assay (Bessey *et al.* 1946), which are sensible methods for evaluation of HOB, were used to measure the rates of cell proliferation and differentiation, respectively, after 1, 4, 7 and 10 days of culture. The control C-s-HA sample was tested only after 10 days.

2.7.1. Cell proliferation (Alamar Blue assay). Alamar Blue solution (Alamar Biosciences, Inc.) was added to the culture medium at each sampling point at 10 vol% and cultured in a humidified incubator for 3 h. Thereafter, 1 ml samples of the culture were added to a 24-well plate and the fluorescent intensities were measured using a microplate reader, with fluorescence excitation and emission wavelengths of 544 and 590 nm, respectively, in order to compare the cell-proliferation rates. The culture was discontinued after the Alamar Blue assay had been performed.

2.7.2. Cell differentiation (ALP assay). ALP activity was measured using an Alkaline Phosphor B assay (Wako Pure Chemical Industries, Ltd). A 1 ml sample of *p*-nitrophenyl phosphoric-acid buffer solution was added and reacted for 1 h at 37 °C, then terminated by 1 ml of 0.02 N NaOH aqueous solution. The absorbance of 0.1 ml of each sample solution was measured on a 96-well microplate at 405 nm using a microplate reader. The ALP activity was determined after accounting for *p*-nitrophenol (pNP) through the calibration curve by subtracting the blank value.

2.8. Three-dimensional HOB development

After 7 days of culture, the HOBs were fixed on the cellular cubic composites (C-u-HA70 and C-β-TCP70, which showed good cell affinity) by treating them with 4% paraformaldehyde for 15 min at room temperature. After fixation, the cellular cubic composites were dehydrated in serial concentrations of ethanol (30, 50, 70, 80, 90 and 100% v/v) for 2 days each, after which they were embedded in LR White embedding resin (London Resin Company Ltd). Horizontal sections were cut with a band saw (BS-3000CP, EXAKT cutting system) perpendicular to the disc and polished with diamond paper. Sections (approx. 20 μm thickness) were then stained with hematoxylin-eosin (H&E) and observed under a BX51 light microscope (Olympus Corp.). Unseeded C-u-HA70 and C-β-TCP70 were also stained with H&E as controls.

2.9. Animal experiments

2.9.1. Extra-osseous implantation. C-u-HA70 and C-P(D/L)LA-only (control) cylinders (∅6.0 mm × 15 mm) were used to demonstrate the osteoinductive properties of the materials themselves.

Six mature beagles (Kitayama Labes Co., Ltd, Nagano, Japan), with average body weights (BWs) of 9.5–11.0 kg, were used in this study. The animals were reared and the experiments were performed at the Institute of Laboratory Animals, Faculty of Medicine, Kyoto University, Japan. All procedures were carried out in accordance with the Guidelines for Animal Experimentation of Kyoto University after the procedures have gained ethical approval. The dogs were anesthetized by intramuscular administration of xylazine (Bayer, Germany; 6.0 mg kg^{-1} BW) and ketamine hydrochloride (15 mg kg^{-1} BW), and local administration of 0.5% (w/v) lidocaine. Surgery was performed under standard aseptic conditions. After the skin and fascia had been incised, pouches were carefully made in the dorsal muscle of the back. Each material was implanted into a separate pouch to prevent inter-sample contact. No additional osteogenic cells or cytokines were provided. A total of 13 samples were implanted and the cylinders were retrieved 1 month (three samples), 6 weeks (three samples), 2 months (three samples), 3 months (three samples) and 12 months (one sample) after implantation.

2.9.2. Histological examination. The retrieved cylinders were fixed in 10% phosphate-buffered formalin for 7 days. One-half of each cylinder was then decalcified, embedded in paraffin, sectioned perpendicular to its axis and stained with H&E. The other half of each cylinder was undecalcified and dehydrated in serial concentrations of ethanol (30, 50, 70, 80, 90 and 100% v/v; 2 days for each concentration) and then embedded in LR White resin (London Resin Company Ltd). The specimens were sectioned using a band saw (BS-3000CP, EXAKT cutting system) perpendicular to the axis of the cylinder. The cross-sectional surface

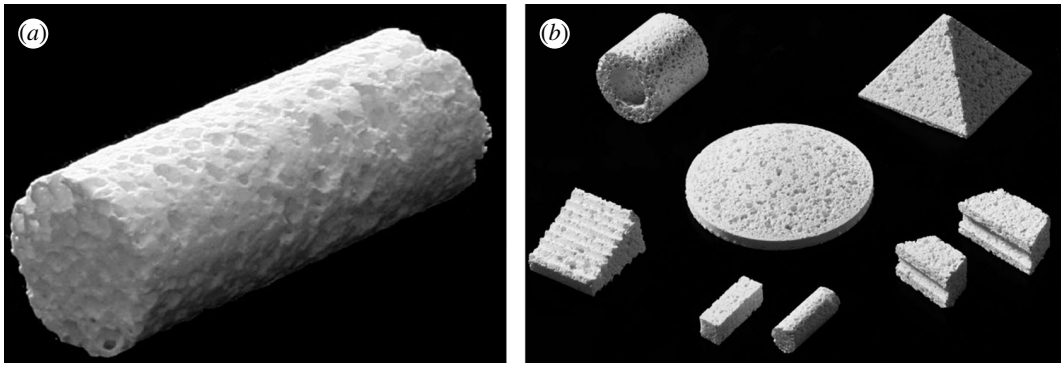

Figure 1. (*a*) Representative cylindrical block of C-β-TCP70. (*b*) Customized blocks of C-u-HA70 (Comporus).

Table 3. Sc values of cellular cubic composites with different u-HA contents.

	u-HA/P(D/L)LA (wt ratio)				
	0/100[a]	50/50	60/40	70/30	80/20
Sc (MPa)	7.3±0.4	6.5±0.3	5.6±0.7	4.1±0.4	1.5±0.2

[a] The interconnective porosity was 45–50% with an 110 μm average pore size.

was polished with diamond paper, subjected to Villanueva Goldner staining (Villanueva & Mehr 1977) and observed under a light microscope.

The areas of ectopic bone (including bone-marrow tissue), which stained green with the Villanueva Goldner stain, were calculated using the IMAGE-PRO Plus program (Media Cybernetics, Inc.). For each sample, the ratio of the green-stained area to the total cross-sectional area of an intact cylinder was calculated using the following equation:

$$\text{area (\%) of ectopic bone} = \left(\frac{\text{green-stained area within a disk}}{\text{area of intact disk with a 6 mm diameter}}\right) \times 100.$$

2.10. Statistical analysis

The Student's *t*-test was used for all statistical analyses.

3. RESULTS

3.1. Mechanical and cellular properties

Figure 1*a* shows a representative cylindrical block of C-β-TCP 70 (∅6.0×15 mm). Blocks of C-u-HA70, C-β-TCP 70 and C-OCP50 were used to measure the changes in $\overline{\text{Mv}}$ and Sc values over time. In addition, the profiles of various cubes of C-u-HA70 were customized as shown in figure 1*b*.

Varying the fraction of u-HA particles in u-HA/P(D/L)LA from 50 to 80 wt% caused changes in mechanical strength (table 3). The Sc value of C-u-HA70 was dependent upon the CaP-particle content and reached a critical point at 70 wt%, which was comparable to that reported for natural cancellous bone (Kasplan *et al.* 1994). Thus, a porosity of 70% was chosen for all of the cellular cubic composites, with the exception of C-OCP50, in order to achieve the desired effects on cell proliferation and differentiation (Kondo *et al.* 2005). The Sc value also increased depending upon the primary-crystal form of the CaP particles (in the order spheroid > hexagonal columnar > lamellar) and, to a lesser extent, the density (tables 1 and 4). Figure 2 shows SEM images of the inner pores of cellular cubic composites containing 70 wt% of the six types of CaP particle in P(D/L)LA, 50 wt% of OCP in P(D/L)LA, 70 wt% of u-HA in PGA/(D/L)LA and cancellous bone from a canine distal tibia as a control. All of the cellular cubic composites, with the exception of C-u-HA70LG, had a similar interconnective cellular structure to that of cancellous bone. The anomalous result for C-u-HA70LG was probably due to its poor solubility in standard solvents. As shown in figure 3, the macro-pores decreased in size as the u-HA content varied from 50 to 70 wt%, and were noticeably smaller at 80 wt%. We therefore determined the critical concentration for practical porosity to be 70 wt%. The cellular geometry of u-HA/P(D/L)LA changed depending upon the u-HA content; at values ranging from 50 to 70 wt% the composites resembled cancellous bone, although some larger pores were created when the specimens were cracked to prepare samples for SEM (figures 2 and 3). In general, the cellular cubic-composite pores ranged in size from 40 to 600 μm (average = 130–250 μm; table 4). However, subsets of considerably smaller pores, ranging in size from 0.05 to 1 μm (average = 0.23 μm), were present in C-u-HA70 (figure 4); the latter were located in the cell walls (figures 2 and 3). The fraction of the interconnective porosity within the total porosity of C-u-HA70 was greater than or equal to 70%. Previously, cellular sintered CaP bioceramics have been reported to require a porosity of greater than 75% (Kondo *et al.* 2005) and a pore size of 100–600 μm (Jarcho 1981; Flatley *et al.* 1983; Kawamura *et al.* 1987; Eggli *et al.* 1988; Passuti *et al.* 1989; Ishaug-Riley *et al.* 1997; Yuan *et al.* 1999) in order to be effective in terms of cell culture and bone ingrowth (Yuan *et al.* 1999).

The average sizes of the macro-pores in the cellular cubic composites varied in the following order: C-β-TCP70 > C-α-TCP70 > C-u-HA70, C-Te CP70, C-DCPA70 and C-DCPD70 > C-OCP50 > C-u-HA70LG. Minor differences in the sizes and the geometrical structures of the pores might have resulted from differences in the primary crystal forms of the CaP particles. C-u-HA70 had relatively small macro-pores

Table 4. Sc values and porosities of cellular cubic composites.

				mechanical and porosity properties of composites		
abbreviation of cellular cubic composite	composition[a]	weight ratio (w/w)	volume ratio (v/v)	average pore size[b] (μm)	distribution of macro-pore size[b] (μm)	Sc (MPa)
C-u-HA70	u-HA/P(D/L)LA	70/30	51.9/48.1	170	40–480	4.1±0.4
C-α-TCP70	α-TCP/P(D/L)LA	70/30	50.4/49.6	200	40–600	5.8±0.6
C-β-TCP70	β-TCP/P(D/L)LA	70/30	48.7/51.3	250	40–600	5.4±0.5
C-TeCP70	TeCP/P(D/L)LA	70/30	46.4/53.4	240	40–600	5.5±0.6
C-DCPA70	DCPA/P(D/L)LA	70/30	55.1/44.9	210	40–600	3.0±0.3
C-DCPD70	DCPD/P(D/L)LA	70/30	49.9/50.1	220	40–600	2.9±0.1
C-OCP50	OCP/P(D/L)LA	50/50	31.9/68.1	130	40–400	3.1±0.2
C-u-HA70LG	u-HA/PGA/(D/L)LA	70/30	51.9/48.1	100	40–300	2.7±0.2

[a] (D/L) =50/50, (LA/GA) =15/85 mol%.
[b] Average pore size and distribution of macro-pores were measured using μCT.

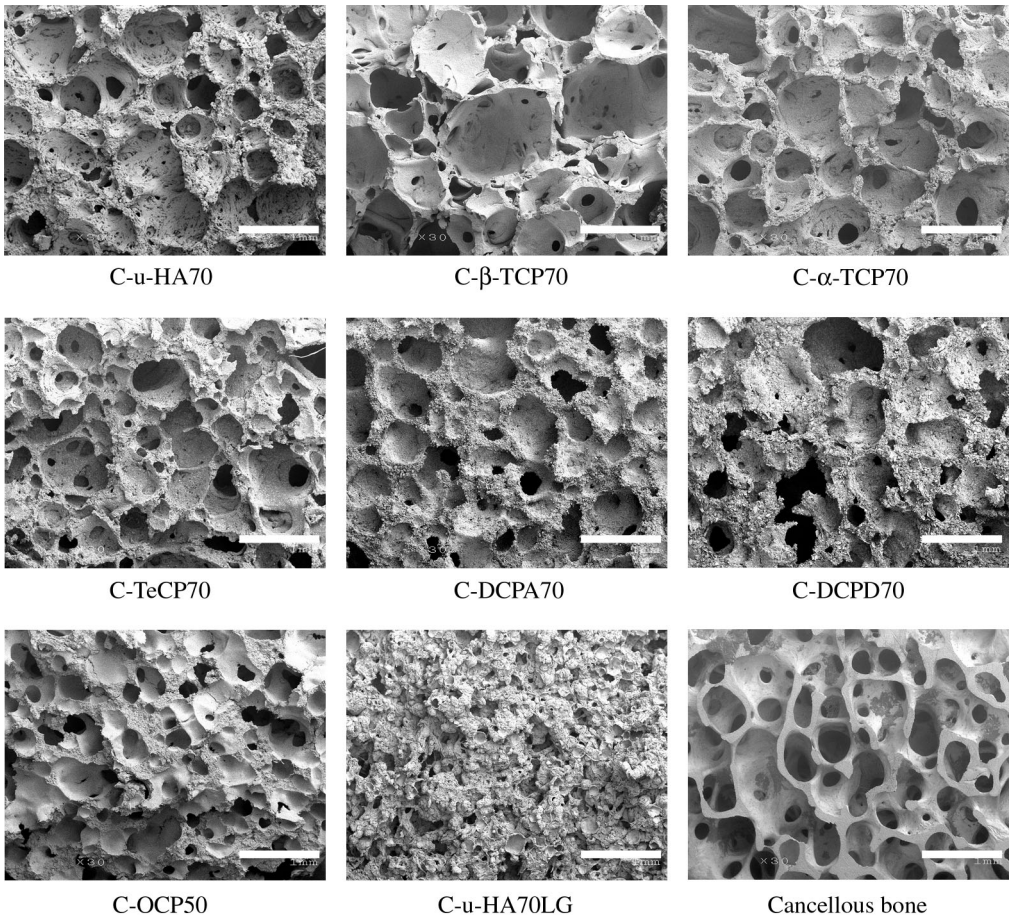

Figure 2. SEM images of the inner pores of CaP particle/P(D/L)LA cellular cubic composites and cancellous bone of a beagle distal tibia (original magnification ×30; scale bar, 1 mm).

and numerous submicron-sized cells within its walls. C-β-TCP70, C-TeCP70 and C-OCP50 had fewer submicron-sized pores, while C-DCPA70 and C-DCPD70 had the least numbers of such pores. C-α-TCP70 exhibited an intermediate condition. Its cellular construction resembled that of C-u-HA50, but it lacked submicron-sized pores in the walls. Moreover, cancellous bone of the canine distal tibia had a higher porosity and fewer smaller submicron-sized pores in the cell walls than C-u-HA70.

The P(D/L)LA-only material fabricated by the CFP method had a porosity of 63–70%, a relatively small macro-pore size (range=40–400 μm; average=110 μm) and a closed cell ratio of 50–55%. Its Sc value was the highest among the materials tested, due to the elasticity of the closed air-containing cells. C-s-HA had a porosity of approximately 50% and a relatively small pore size (range=5–100 μm). Four cellular cubic composites (C-β-TCP70, C-u-HA70, C-DCPD70 and C-TeCP70), each with a CaP-particle content of

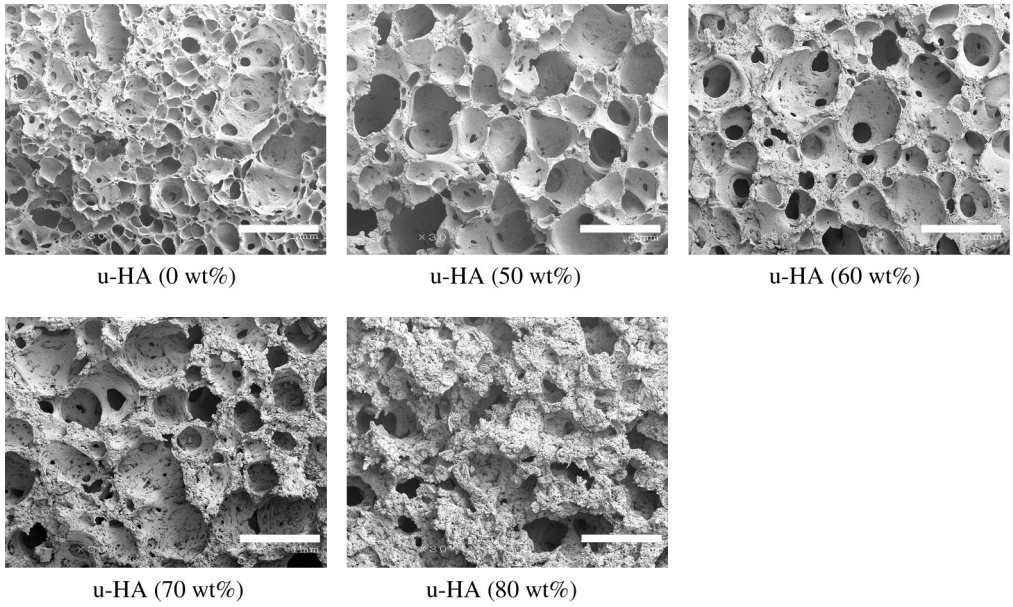

Figure 3. SEM images of inner pores of u-HA/P(D/L)LA cellular cubic composites with different u-HA contents (original magnification ×30; scale bar, 1 mm).

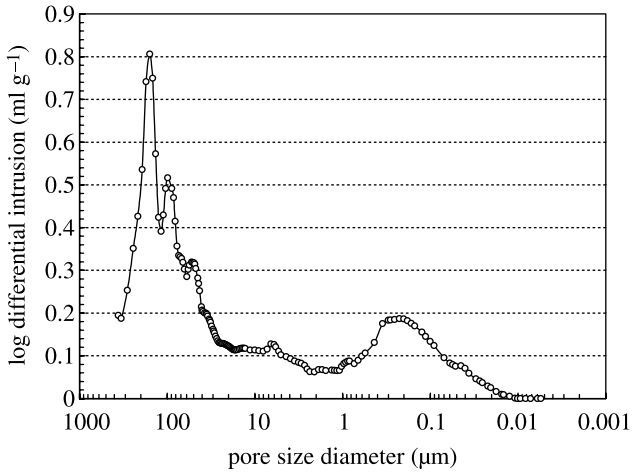

Figure 4. Pore-size distribution in C-u-HA70.

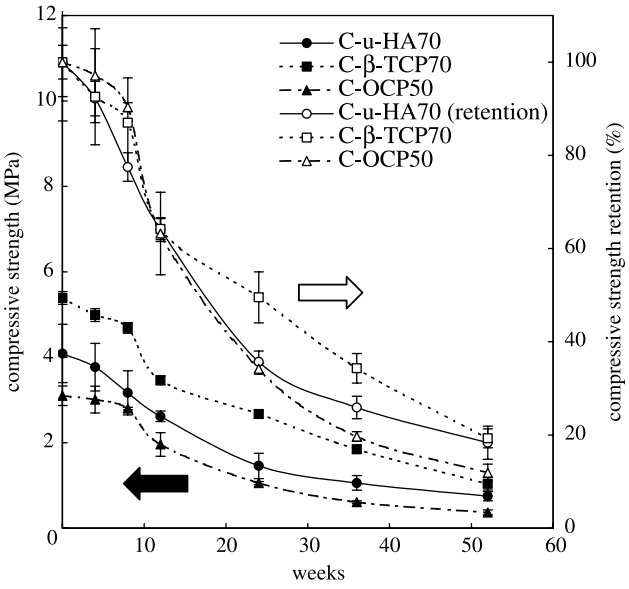

Figure 6. Changes in Sc values of C-u-HA70, C-β-TCP70 and C-OCP50 over time in SBF at 37 °C. The symbols filled circle, filled square and filled triangle denote Sc, whereas open circle, open square and open triangle denote Sc retention.

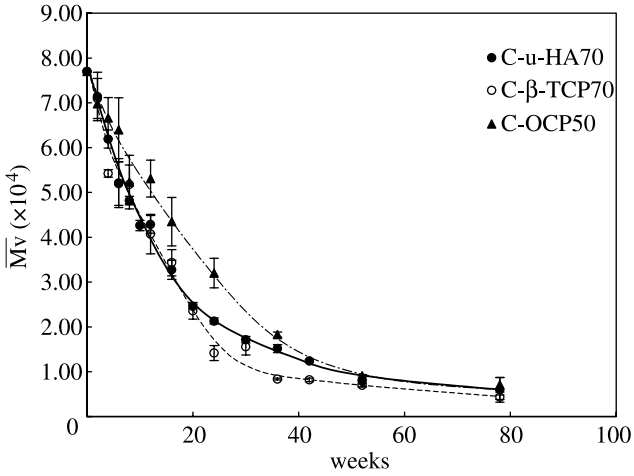

Figure 5. Changes in $\overline{\mathrm{Mv}}$ values of C-u-HA70, C-β-TCP70 and C-OCP50 over time in SBF at 37 °C.

70 wt% and a porosity of 70%, were used in the cell-culture tests of porosity, pore geometry, physical strength, bioactivity and bioresorbability.

3.2. Changes in $\overline{Mv}$ and Sc in vitro

Figure 5 shows the *in vitro* $\overline{\mathrm{Mv}}$ changes in SBF without stirring or replacement. The $\overline{\mathrm{Mv}}$ values of C-u-HA70, C-β-TCP70 and C-OCP50 were similar for the first 52 weeks. Thereafter, from 52 to 78 weeks (1–1.5 years), the values decreased to approximately 10–5 kDa and stirring tended to break the materials into micro-sized fragments. We predict that these materials might be replaced with natural bone within approximately 1.5 years under

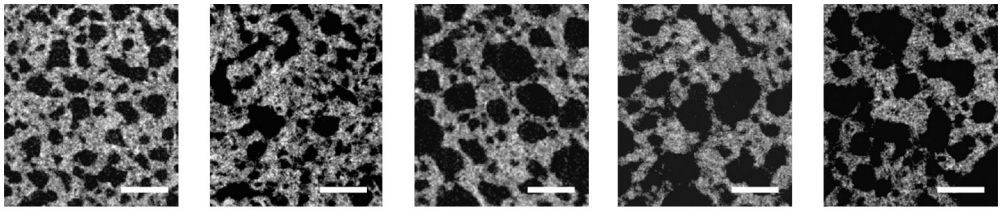

	(a) 0 (intact)	(b) 12	(c) 20	(d) 36	(e) 52
weeks					
maximum pore size (μm)	~480	~550	~570	~600	~700

Figure 7. *In vitro* cellular changes in C-u-HA70 under μCT with time (original magnification ×30; scale bar, 500 μm).

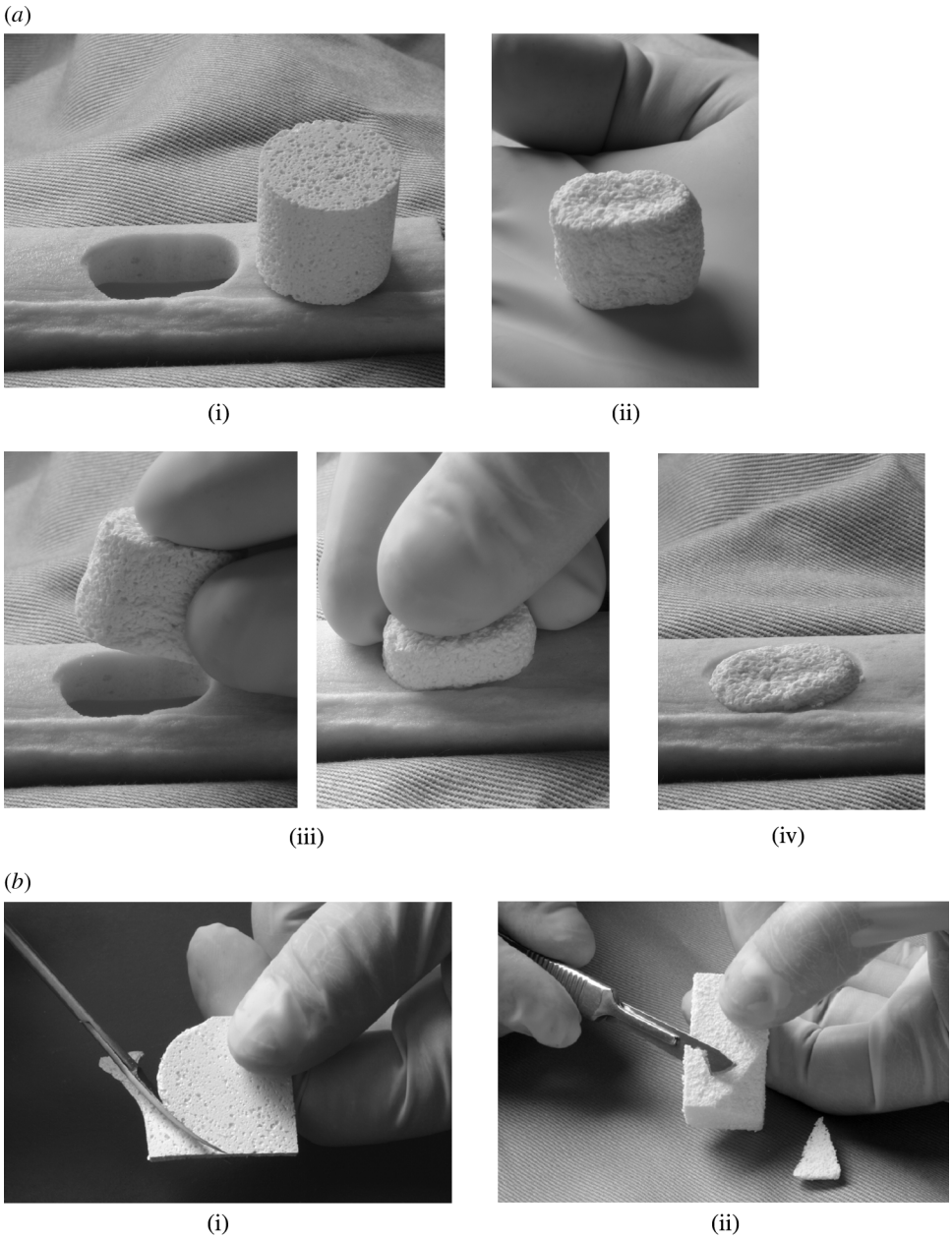

Figure 8. Intraoperative transformation and trimming procedures for C-u-HA70. (*a*) Transformation and insertion procedures: (i) a Comporus C-u-HA70 cylinder (ø18× H 18 mm) and a hole of rectangle with rounded ends in an artificial bone (minor axis = 16 mm); (ii) the transformed oval column after heating at 65 °C; (iii) insertion of the column into the defect and (iv) the column set in the artificial bone. (*b*) Trimming procedures: (i) a square Comporus C-u-HA70 plate being trimmed into a round sheet using operating scissors; (ii) removal of the edges of a Comporus C-u-HA70 block by shaving with a scalpel.

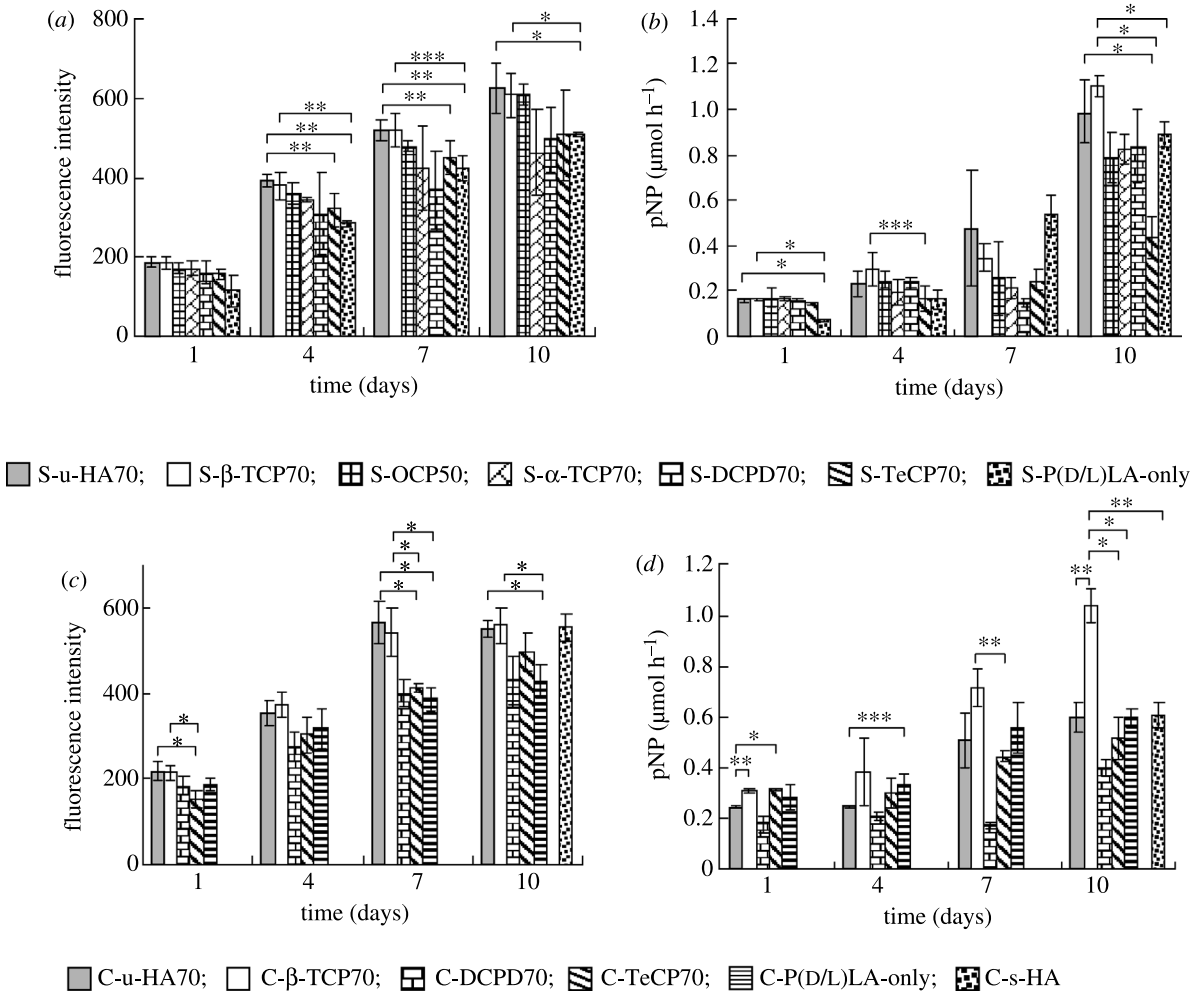

Figure 9. Alamar Blue assay (fluorescence excitation wavelength, 544 nm; fluorescence emission wavelength, 590 nm) of HOBs in (*a*) sheet composites and (*c*) cellular cubic composites, and ALP activities of HOBs in (*b*) sheet composites and (*d*) cellular cubic composites, over 10 days. $^{*}p<0.005$; $^{**}p<0.01$; $^{***}p<0.05$.

in vivo loading conditions, although this will vary depending upon the size and initial $\overline{\text{Mv}}$ value of each device. Interestingly, a P(D/L)LA sample with an initial $\overline{\text{Mv}}$ of 15 kDa was previously reported to achieve complete mass loss *in vitro* after 1 year (Mooney *et al.* 1995). In the current study, a P(D/L)LA sample with an initial $\overline{\text{Mv}}$ of 77 kDa decreased to an equivalent value after approximately six months, and thereafter took approximately 1 year to reach a minimum $\overline{\text{Mv}}$ of approximately 5 kDa. Both studies therefore showed similar degradation rates. The addition of osseous growth factors could significantly shorten the period of time required for replacement with natural bone.

The initial Sc values (mean$\pm$s.d.) for C-β-TCP70 and C-OCP50, as described in table 4, can be explained, respectively, by the presence of β-TCP particles at the lowest volume (highest density) and by the lamellar form of the OCP crystals, which might make the composite difficult to reinforce at greater than or equal to 50 wt%. C-u-HA70 had an intermediate Sc value (4.1 ± 0.4), which remained within the range seen in natural cancellous bone (1.9–7.0 MPa; Lotz *et al.* 1990) even after 20 weeks in SBF (figure 6).

The aforementioned Sc values are sufficient for use in scaffolds for bone reconstruction or as bone substitutes, provided that the cellular cubic composites are reinforced by hybridization with high-strength cancellous bone-like bioactive and bioresorbable devices (as detailed in §3.8).

3.3. Porosity changes in vitro

The initial maximum cell size (480 μm) of C-u-HA70 increased to approximately 700 μm after 52 weeks, while the numbers of micro-sized cells decreased significantly due to *in vitro* dissolution and dispersion into the SBF. These processes resulted from the collapse of the cell walls caused by P(D/L)LA hydrolytic degradation over time (figure 7).

3.4. Intraoperative trimming and heat transformation

Figure 8 demonstrates that C-u-HA70 could be both heat-transformed and trimmed, in order to adapt its shape to that of the defect. This was due to the plasticity of the amorphous P(D/L)LA, which occupied 30 wt% (50 vol%) of the composite. Transformation at a temperature just above T_g did not cause fusion of the P(D/L)LA, and the pore geometry was almost preserved but deformed the original pore shape only, thereby retaining an effective pore size for bone ingrowth.

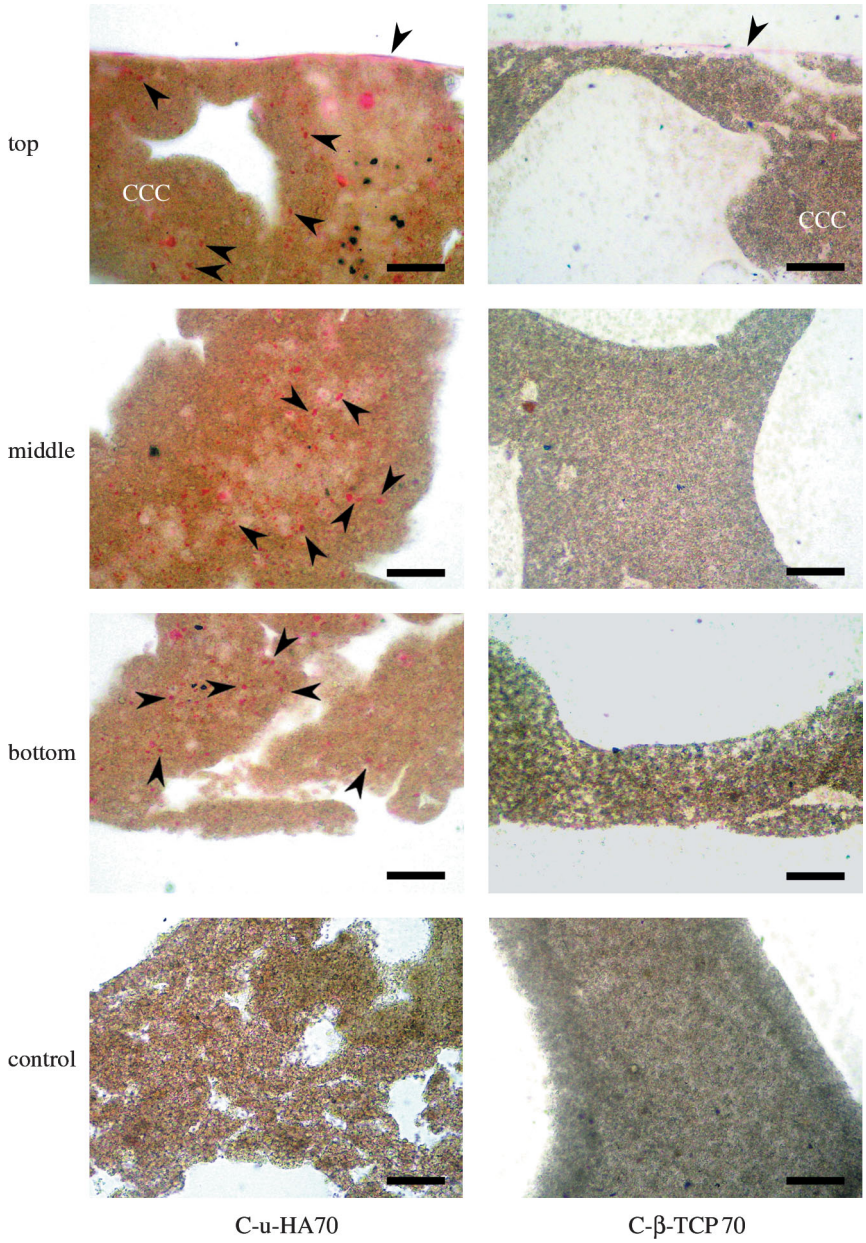

Figure 10. Microscopic H&E-stained images of HOBs cultured on C-u-HA70 and C-β-TCP70 for 7 days. Arrowheads indicate HOBs (original magnification ×200; scale bar, 50 μm). HOBs were not seeded in the controls. As the organic solvent to get rid of the resin dissolves these cellular cubic composites, the sections were stained with H&E while embedded in resin. The HOBs therefore appeared to be lightly stained.

3.5. Osteoblast affinity

The results of the Alamar Blue and ALP assays of cell proliferation and differentiation in the non-porous sheet composites are shown in figure 9*a*,*b*, respectively. The corresponding data for the cellular cubic composites are shown in figure 9*c*,*d*, respectively.

Based on these results, we were able to ascertain the differences between the two- and three-dimensional osteoblast affinity of the composites, as detailed below.

3.5.1. Cell proliferation of sheet composites. The number of HOBs in each sheet composite increased over 10 days of culture. The cell-proliferation rates in S-u-HA70, S-β-TCP70 and S-OCP50 were significantly greater than those in S-α-TCP70, S-DCPD70 and S-TeCP70. The S-P(D/L)LA-only sample showed the lowest rate of HOB proliferation (figure 9*a*).

3.5.2. Cell differentiation of sheet composites. The ALP activity of each sheet composite increased significantly after 10 days of culture. By contrast, the ALP activity of the S-P(D/L)LA-only sample showed a drastic increase after just 7 days. The cell-growth rate might have been higher in the S-P(D/L)LA-only material during the early stages of the culture period, thereby inducing the cells to progress to the differentiation stage, because the potential for cell proliferation was relatively low. S-u-HA70 and S-β-TCP70 showed the highest ALP activities in HOBs (figure 9*b*).

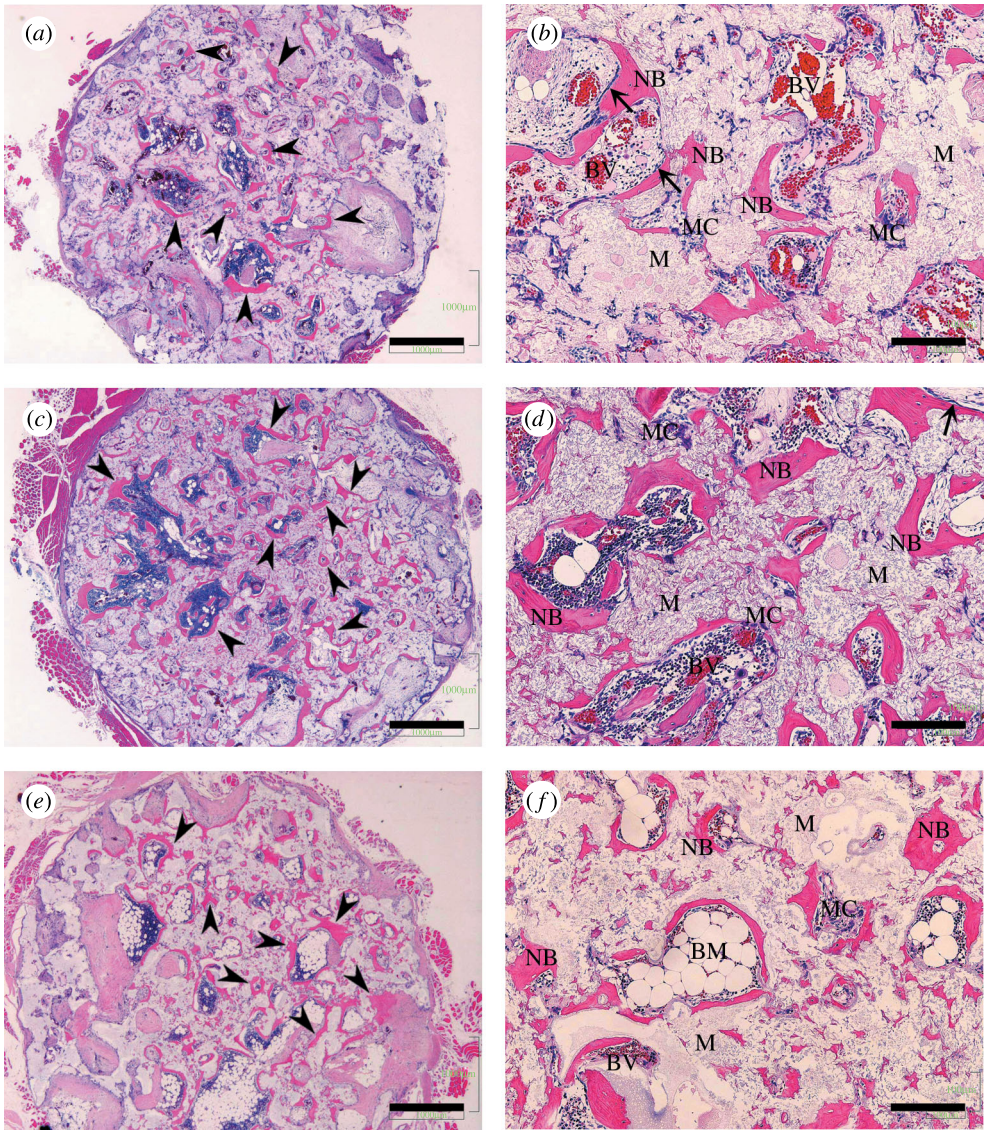

Figure 11. H&E staining of decalcified sections. Ectopic bone formation (arrow heads) was seen in the pores of C-u-HA70. Osteoblast-like cells (arrow) were detected adjacent to the newly formed bone. (*a*) and (*b*) Two months after implantation of C-u-HA70; (*c*) and (*d*) Three months after implantation of C-u-HA70; (*e*) and (*f*) Twelve months after implantation of C-u-HA70. (*a*), (*c*) and (*e*) Original magnification ×20; scale bar, 1 mm. (*b*), (*d*) and (*f*) Original magnification ×100; scale bar, 200 μm; BM, bone-marrow tissue; BV, blood vessel; M, material; MC, multinucleated cell; NB, newly formed bone.

3.5.3. Cell proliferation of cellular cubic composites. The number of HOBs in all the cellular cubic composites increased over time (figure 9*c*). However, only C-u-HA70 and C-β-TCP70 reached a plateau after 7 days, probably because cell confluence had been achieved. The cell-proliferation rates in C-u-HA70 and C-β-TCP70 were significantly greater than those in C-DCPD70 and C-TeCP70 at 7 days, and the HOB-proliferation rate in the C-P(D/L)LA-only material was significantly lower than those in both C-u-HA70 and C-β-TCP70 after 7 days. The HOB-proliferation rates in C-u-HA70 and C-β-TCP70 after 10 days were significantly greater than those in the other cellular cubic composites, and were similar to those in the C-s-HA-only material. Overall, C-u-HA70 and C-β-TCP70 showed the greatest HOB-proliferation capacities.

3.5.4. Cell differentiation of cellular cubic composites. The ALP activity of C-β-TCP70 was higher than that of C-u-HA70 and the other composite materials (figure 9*d*). This was probably due to differences in their three-dimensional cellular and cell-wall structures. In particular, although the average pore sizes of C-u-HA70 and C-β-TCP70 were similar (170 and 250 μm, respectively), the latter lacked submicron-sized pores in the cell walls; thus, the total inner surface area of pores of C-β-TCP70 was smaller than that of C-u-HA70, and the transition to cell differentiation after reaching cell confluence was faster. The ALP activity of C-u-HA70 was comparable to that of C-s-HA after 10 days, and was similar to that of the C-P(D/L)LA-only material at both 7 and 10 days. As discussed above, cells in the C-P(D/L)LA-only material proliferated and reached saturation relatively early during culture.

C-u-HA70 and C-β-TCP70 had distinctive HOB affinities and growth rates compared with the other cellular cubic composites. However, our examinations were conducted over a relatively short period (10 days). During longer periods (for example, 1 year), the

P(D/L)LA should be largely resorbed *in vivo*. Therefore, our present results might differ from those seen in clinical cases. We previously confirmed that C-u-HA70 promoted osteoconductive bone ingrowth after 1.5 months (Hasegawa *et al.* 2005*a*), which highlighted one difference between *ex vivo* and animal-implantation studies.

3.6. Three-dimensional HOB development

Figure 10 compares the three-dimensional infiltration behaviour of HOBs (at a concentration of 1.0×10^5 cells ml^{-1}) into C-u-HA70 and C-β-TCP70 after 7 days. Red-stained HOB cells (black arrows), along with micro/macro-sized and submicron-sized cells, densely infiltrated the cell walls of C-u-HA70. By contrast, these cells less densely infiltrated C-β-TCP70 and its cell walls. Differences in pore condition and size distribution might affect cell proliferation and differentiation. This supports the hypothesis that an early shift to cell differentiation occurs in C-β-TCP70, which shows relatively high ALP activity compared with C-u-HA70.

3.7. Intramuscular implantation

The results of the histological examinations of intramuscular implants after 2, 3 and 12 months are shown in figure 11. The findings clearly illustrated osteoinductive bone formation by C-u-HA70 itself. The H&E-stained sections revealed neither ossification nor bone formation in the three specimens after 1 and 1.5 months. However, distinct bone formation was observed after two months and ectopic bone formation was observed in two of the three specimens retrieved at this point of time. Neither chondrocytes nor cartilage-like tissues were seen on the materials or in their pores. However, newly formed bone and multinucleated cells were observed adjacent to the materials. Moreover, osteoblast-like cells were found adjacent to the newly formed bone, which might have exhibited intramembranous ossification. In all of the three specimens retrieved after three months, ectopic bone formation was present similarly to that observed two months after implantation. However, the amounts of newly formed bone in the pores showed individual differences. After 1 year, the newly formed bone had been remodelled and bone-marrow formation was observed in the pores of the one remaining specimen. The osteoblast-like cells that had been observed adjacent to the newly formed bone after two months were absent. No signs of infection, inflammatory reaction or severe foreign-body reaction were noted during the observation period. No obvious osteogenesis was detected on or in the porous C-P(D/L)LA-only material during the study period.

Figure 12 shows light-microscopy images produced with Villanueva Goldner staining. The proportions of new bone, which were visible by their green staining, were 8.5 and 38.1% after 3 and 12 months, respectively.

C-u-HA70 itself showed osteoinductivity that persisted even after 12 months and the amount of newly formed bone in the pores was much greater than that observed after three months. This was probably due to the absorption of the degraded P(D/L)LA, which increased the ratio of u-HA particles as they were exposed from the matrix.

3.8. Potential applications

Figure 13 shows four potential hybrid-type cortico-cancellous bone substitutes and scaffolds designed for the reconstruction of hard tissues. These composites have been combined with high-strength cortical bone-like bioactive and bioresorbable devices, such as OSTEOTRANS (u-HA/PLLA = 40 : 60 weight ratio; Shikinami & Okuno 1999; Shikinami *et al.* 2005), and C-u-HA70.

OSTEOTRANS is an osteoconductive and bioresorbable bone-fixation device which has high initial mechanical strength compared with natural cortical bone that persists for six months or more. By contrast, C-u-HA70 allows osteoconduction and osteoinduction (as described above). These hybrid-type cortico-cancellous bone substitutes and scaffolds can retain the strengths provided by OSTEOTRANS for sufficient periods of time, while the C-u-HA70 allows new bone ingrowth through its osteoinductivity. Both materials are gradually absorbed and eventually replaced with natural bone, in order to realize complete hard-tissue reconstruction, even for large defects produced by surgical debridement. Furthermore, impregnating biological growth factors into C-u-HA70 might remarkably enhance the regeneration and reconstruction of hard tissues.

Figure 13*a* shows an incurvate hybrid-fusion cage designed for use as a vertebral spacer, which would bond to the disc bodies and be gradually replaced with natural bone. This device could be used as a partial prosthetic lumbar disc for interbody fusion with a posterior approach. Figure 13*b* shows a hybrid vertebral spacer designed for use in total lumbar fusion with an anterior approach, which would be more reliable in terms of performance and sterilization than the existing lumbar-allograft systems. Figure 13*c* shows a hybrid hook wedge designed to be used in high tibial valgus osteotomy for compartment osteoarthritis of the knee, which could replace the fragile s-HA devices that are currently employed. Finally, figure 13*d* shows a novel customized hybrid mesh tray with mini-screws for fixation to adjoining intact bone around a C-u-HA70 block, which could be customized for application to large mandibular defects.

4. DISCUSSION

4.1. Design of optimal porous-composite scaffolds

Even for cell scaffolds designed as temporary implants, superior results might be achieved if they are composed of a 'biomimetic' material that mimics the chemical composition and cellular morphology of living tissue. Numerous important issues must therefore be considered when developing bioactive and bioresorbable porous composites for clinical use as cell scaffolds.

For example, both the components of a composite (i.e. the bioactive CaP particle and the matrix polymer) must be bioresorbable in order to allow total replacement by natural tissues, and, more importantly, to avoid inflammatory and cytotoxic reactions (Shikinami *et al.* 2005).

In addition, the CaP particle that reinforces the matrix polymer must be chosen carefully to ensure that it is present at a suitable ratio within the composite, and displays optimal three-dimensional cell affinity leading to strong bioactivity. Nano-sized particles tend to be present at high volumes and have large surface areas.

Despite the numerous studies that have investigated the use of nano-particles in biomaterials, it remains unclear whether the inclusion of high volumes of nano-sized particles within polymers has a significant effect on mechanical strength and/or cytotoxicity. We therefore recommend designing composites with slightly larger CaP particles, such as those used in the current study. The CaP-particle size employed in the current cellular cubic composites (3–5 μm on average) appeared to result in an acceptable resorption rate and satisfactory levels of biological safety and bioactivity. A value of greater than or equal to 50 vol% allowed the serial connection of CaP particles to occur throughout the substance and the exposure of CaP particles on the total surface of C-u-HA70, and provided good three-dimensional cell affinity and bioactivity, while a value of greater than or equal to 70 wt% provided physical reinforcement and increased rigidity. Incidentally, natural cancellous bone comprises approximately 70 wt% CaP particles and approximately 30 wt% collagenous matrix in the dry condition (Kasplan *et al.* 1994). A cellular geometry with greater than or equal to 70% porosity, including greater than or equal to 70% interconnective pores, leads to strong bioactivity coupled with bone ingrowth through interconnective pathways.

Finally, amorphous P(D/L)LA is a convenient polymer in terms of its solubility in standard volatile solvents. This is an important consideration when applying the CFP method and for ensuring an adequate degradation rate *in vivo*.

4.2. Production process

Numerous production processes have been developed for open-cell porous industrial materials and biomaterials. These include the following: the sublimation method, which involves freeze-drying polymer solutions; filler (porogen)-eluting (leaching) methods; sintering and depositing methods that utilize microcrystals or particles; the three-dimensional-printing process (Griffith *et al.* 1997); and foaming methods employing supercritical CO_2 (Montjovent *et al.* 2005) and liquid-chemical reactions, such as the polyurethane reaction. However, these approaches have so far failed to produce interconnective porous composites comprising CaP particles (greater than or equal to 50 vol%, greater than or equal to 70 wt%) within an organic bioresorbable polymer matrix, even though various types of porous composite scaffold have been investigated (Rezwan *et al.* 2006). This is mainly due to the difficulty involved in obtaining homogeneous composites at the viscosities required to produce cellular materials, as well as the fragile nature of highly porous composites (compressive strength less than 0.5 MPa; Guan & Davies (2004)).

Our novel CFP method has solved these problems by allowing the bioactivity on the large total surface area of the CaP particles in matrix polymers to be exploited while the materials degrade. The cellular cubic composites produced using our method possess all the properties previously described as vital in optimal hard-tissue scaffolds. The morphology of C-u-HA70 results in optimal bioactivity (in terms of the three-dimensional cell affinity, osteoconductivity and osteoinductivity), and a comparable Sc value and cellular geometry to those of cancellous bone. Moreover, the plasticity of the polymer matrix ensures that it can be manipulated intraoperatively.

4.3. Advantages of cellular cubic composites

Although various types of polymer-only porous scaffold have been proposed previously, none have shown sufficient hard-tissue affinity (Burdick *et al.* 2003), and suitable chemical surface-modifications have not yet been realized (Vehof *et al.* 2002).

The cellular cubic composites demonstrated in this report have several advantages over existing materials, as summarized below.

First, complete replacement with natural hard tissues can be achieved through the gradual resorption of both components of the composites.

Second, the numerous bioresorbable and osteologically bioactive CaP particles (average size = 3–5 μm) present an extensive surface area with high cell affinity, which can induce ossific bioactivity leading to osteoinduction while the composites are being resorbed.

Third, the high porosity can reduce the total mass of the polymer, which is a foreign material that has to be absorbed *in vivo*.

Fourth, amorphous P(D/L)LA and PGA/(D/L)LA polymers can be rapidly resorbed (after 1 and 0.5 years, respectively; Mooney *et al.* 1995); the replacement of these porous composites with natural hard tissues is achieved significantly faster than that of semi-crystalline PLLA.

Fifth, the materials have a similar cellular construction and size distribution to natural cancellous bone, along with a relatively high fraction of interconnective porosity (greater than or equal to 70%), which might promote ossification.

Sixth, the cellular cubic-composite mechanical strengths are comparable to those of natural cancellous bone, depending upon the intrinsic rigidity of the CaP particle and its crystal form.

Seventh, the three-dimensional cellular substances are suitable for clinical use as scaffolds for bone reconstruction or as temporary substitutes for large musculoskeletal defects, owing to their ability to be manipulated intraoperatively (for example, by heat transformation or trimming).

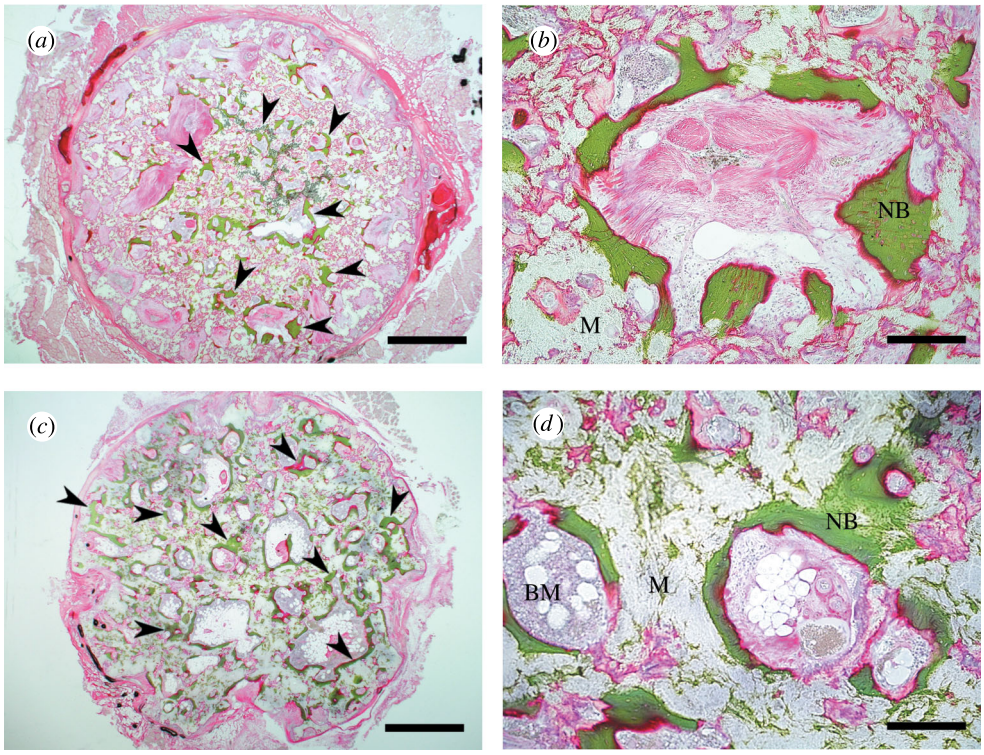

Figure 12. Villanueva Goldner stain of undecalcified sections. Ectopic bone formation (arrow heads) was seen in the pores of C-u-HA70. (*a*) and (*b*) Three months after implantation of C-u-HA70; (*c*) and (*d*) Twelve months after implantation of C-u-HA70. (*a*) and (*c*) Original magnification ×20; scale bar, 1 mm. (*b*) and (*d*) Original magnification ×100; scale bar, 200 μm. BM, bone-marrow tissue; M, material; NB, newly formed bone.

Eighth and finally, the chemical affinity of biological ossific factors for biodegradable matrix polymers, which can either dissolve or swell in volatile standard solvents, could be exploited to design carriers for drug-delivery systems. The controlled release of drugs could be successfully realized by involving ossific factors such as bone-morphogenic protein (BMP), prostanoid receptor EP4 (Sasaoka *et al.* 2004), transforming growth factor-β (TGF-β), platelet-rich plasma (PRP) or basic fibroblast growth factor (b-FGF).

4.4. Differences in cell proliferation/ differentiation among CaP particles

S-β-TCP70 had a stronger cell affinity than S-α-TCP70, despite their similar chemical structures. This might have resulted from differences in their chemical configurations or solubilities. The cell-proliferation rates of C-u-HA70 and C-β-TCP70 were similar, although the latter showed a higher cell-differentiation rate. This was probably caused by differences in their cellular structures. For example, numerous submicron-sized pores were present in the cell walls of C-u-HA70, but not C-β-TCP70, along with macro-sized cells that were smaller than those present in the other cellular cubic composites. In addition, C-β-TCP70 had a smaller inner surface area of pores than that of C-u-HA70, and cell proliferation might have reached saturation earlier and progressed to cell differentiation more rapidly. However, these findings do not necessarily indicate higher ALP activity in β-TCP than in u-HA in general, as this depends upon differences in cellular construction and size distribution.

4.5. Effects of particle surface area on bioactivity

The total surface area of u-HA particles existing in C-u-HA70 was calculated to be 1780 $cm^2\,cm^{-3}$; this was based on the size distribution of the u-HA particles. The total inner surface area of pores in C-u-HA70 (pore size in average =170 μm), which was measured using μCT with the TVIEW program (SkyScan), was 200 $cm^2\,cm^{-3}$ versus 95 $cm^2\,cm^{-3}$ for β-TCP70. The corresponding values for the C-s-HA materials CELLYARD (Pentax Corp.) and BONFIL (Mitsubishi Materials Co., Ltd) were 125 and 111 $cm^2\,cm^{-3}$, respectively. A large surface area (1980 $cm^2\,cm^{-3}$) added up from both surface areas probably affects osteoinduction and osteoconduction during the degradation process.

4.6. Potential osteoinductivity

Ideally, cellular materials for use as scaffolds in bone reconstruction should have osteoconductive and/or osteoinductive activity and should gradually degrade as host tissues replace them. Advanced tissue-engineering technology is currently the best strategy for utilizing natural and artificial carriers for cell transplantation or for the controlled delivery of osteoinductive biological factors. As reported previously (Chang *et al.* 2000; Flautre *et al.* 2001; Hing *et al.* 2004; Mastrogiacomo *et al.* 2006), and confirmed by intramuscular implantation into canine back muscles, C-u-HA70 with a porosity greater than or equal to 75% (Kondo *et al.* 2005) and a pore size of 100–600 μm has excellent

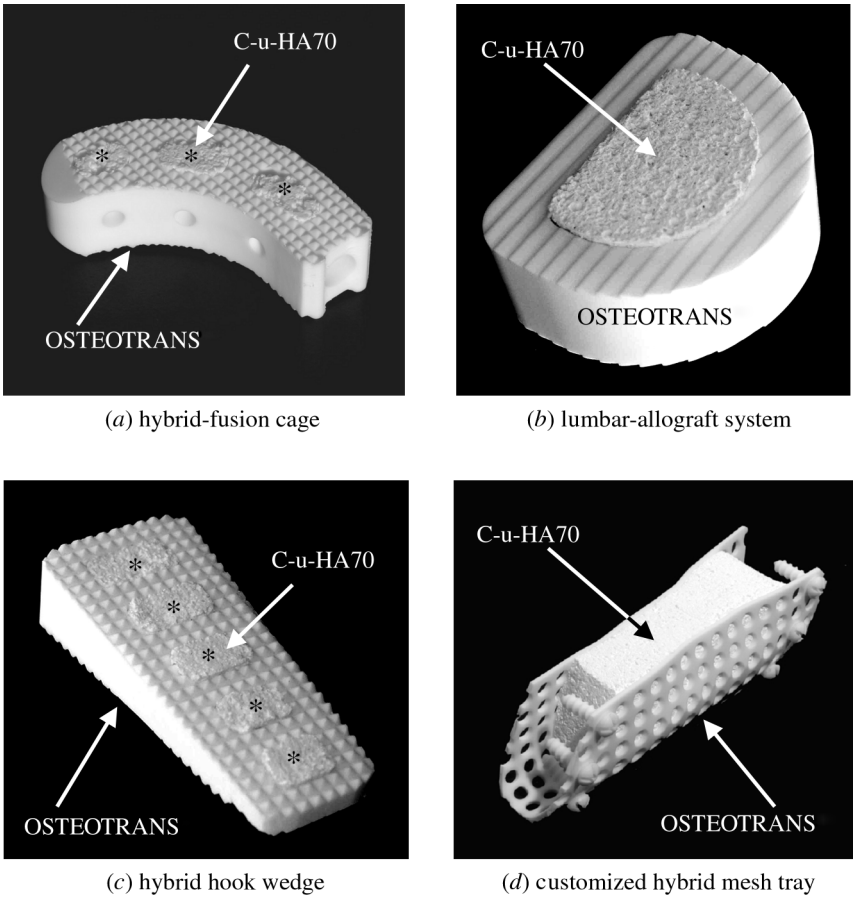

(*a*) hybrid-fusion cage (*b*) lumbar-allograft system

(*c*) hybrid hook wedge (*d*) customized hybrid mesh tray

Figure 13. Hybrid-type bone substitutes and scaffolds. Combinations of C-u-HA70 (Comporus) and OSTEOTRANS (u-HA/PLLA; 40 : 60 wt ratio).

biocompatibility (three-dimensional cell affinity), osteoinductivity and bioresorbability. Moreover, Hasegawa *et al.* (2005*b*) reported that this material induced ectopic osteogenesis in syngeneic rat subculture models, including a model loaded with syngeneic bone-marrow cells. Thus, material-induced osteogenesis clearly occurs, although its mechanism remains unclear. One factor that might influence osteoinductivity is the presence of an appropriate interconnective cellular geometry coupled with a desirable distribution (Yuan *et al.* 1999). Biomaterials with a similar cellular structure to cancellous bone allow fibro-vascular tissues to penetrate into the deeper cellular areas (Tamai *et al.* 2002). It is therefore valid to postulate that an increase in the specific surface area, achieved by introducing micro-pores within the partitioning walls of macro-pores, might induce specific cells to differentiate into an osteogenic lineage, and could thus be essential for osteoinductive activity (Habibovic *et al.* 2005).

The concentrations of Ca and P ions influence osteogenic cells (Quarles *et al.* 1992). The apatite layer surrounding bioactive CaP particles that are fixed by a polymer matrix provides sufficient Ca and P ions during cell differentiation for osteogenesis, and might promote osteoinductivity. Native BMP is also important in osteoinduction processes, and the concentrations of Ca ions can affect BMP adsorption from body fluids (Yuan *et al.* 1998).

Osteoinductivity might require the maintenance of a suitable three-dimensional cellular structure over a sufficient time period (Ripamonti 1996; Kurashina *et al.* 2002). Thus, osteoinductive biodegradable scaffolds should provide a suitable space with three-dimensional stability in order to permit the infiltration of progenitor cells and fibro-vascular tissues. The physicochemical properties of the components of the composites described here might help to maintain favourable Ca and P ion concentrations during biodegradation. Numerous bioactive micro-particles might be exposed on the surface during polymer degradation and this process could generate multiple 'micro-islands' surrounded by high concentrations of Ca and P ions. Moreover, the collapse of the walls between the interconnective pores could expose micro-CaP particles, thereby improving the necessary environment for osteoinduction. In future studies, we intend to investigate the details of the osteoinductive mechanism in the most appropriate cellular cubic composites on a macroscopic scale.

5. CONCLUSIONS

The CFP method can produce bioactive and bioresorbable materials that are suitable for use as cell scaffolds and cancellous bone substitutes. These materials are customizable and are eventually replaced with natural bone. C-u-HA70 and its hybrids, in combination with

artificial cortical bone-like composites (u-HA/PLLA = 40/60 wt ratio), showed the greatest potential for use in bone and cartilage tissue engineering. Furthermore, adding osseous growth factors could significantly shorten the time required for tissue reconstruction and promote the osteoinductivity of C-u-HA70 itself.

REFERENCES

Ahmed, S. A., Gogal Jr, R. M. & Walsh, J. E. 1994 A new rapid and simple non-radioactive assay to monitor and determine the proliferation of lymphocytes: an alternative to [3H]thymidine incorporation assay. *J. Immunol. Methods* **170**, 211–224. (doi:10.1016/0022-1759(94)90396-4)

Bessey, O. A., Lowry, O. H. & Brock, M. J. 1946 A method for the rapid determination of alkaline phosphatase with five cubic millimeters of serum. *J. Biol. Chem.* **164**, 321–329.

Burdick, J. A., Frankel, D., Dernell, W. S. & Anseth, K. S. 2003 An initial investigation of photocurable three-dimensional lactic acid based scaffolds in a critical-sized cranial defect. *Biomaterials* **24**, 1613–1620. (doi:10.1016/S0142-9612(02)00538-0)

Chang, B. S., Lee, C. K., Hong, K. S., Youn, H. J., Ryu, H. S., Chung, S. S. & Park, K. W. 2000 Osteoconduction at porous hydroxyapatite with various pore configurations. *Biomaterials* **21**, 1291–1298. (doi:10.1016/S0142-9612(00)00030-2)

Eggli, P. S., Muller, W. & Schenk, R. K. 1988 Porous hydroxyapatite and tricalcium phosphate cylinders with two different pore size ranges implanted in the cancellous bone of rabbits. A comparative histomorphometric and histologic study of bony ingrowth and implant substitution. *Clin. Orthop. Rel. Res.* **232**, 127–138.

Flatley, T. J., Lynch, K. L. & Benson, M. 1983 Tissue response to implants of calcium phosphate ceramic in the rabbit spine. *Clin. Orthop. Rel. Res.* **179**, 246–252.

Flautre, B., Descamps, M., Delecourt, C., Blary, M. C. & Hardouin, P. 2001 Porous HA ceramics for bone replacement: role of the pores and interconnections-experimental study in the rabbit. *J. Mater. Sci. Mater. Med.* **12**, 679–682. (doi:10.1023/A:1011256107282)

Griffith, L. G., Wu, B., Cima, M. J., Powers, M. J., Chaignaud, B. & Vacanti, J. P. 1997 *In vitro* organogenesis of liver tissue. *Ann. NY Acad. Sci.* **831**, 382–397.

Guan, L. & Davies, J. E. 2004 Preparation and characterization of a highly macroporous biodegradable composite tissue engineering scaffold. *J. Biomed. Mater. Res. A* **71**, 480–487. (doi:10.1002/jbm.a.30173)

Habibovic, P., Yuan, H., van der Valk, C. M., Meijer, G., van Blitterswijk, C. A. & de Groot, K. 2005 3D microenvironment as essential element for osteoinduction by biomaterials. *Biomaterials* **26**, 3565–3575. (doi:10.1016/j.biomaterials.2004.09.056)

Hasegawa, S., Tamura, J., Neo, M., Goto, K., Shikinami, Y., Saito, M., Kita, M. & Nakamura, T. 2005*a* *In vivo* evaluation of a porous hydroxyapatite/poly-DL-lactide composite for use as a bone substitute. *J. Biomed. Mater. Res. A* **75**, 567–579.

Hasegawa, S., Tamura, J., Neo, M., Fujibayashi, S., Goto, K., Shikinami, Y., Okazaki, K. & Nakamura, T. 2005*b* *In vivo* evaluation of porous hydroxyapatite/poly-D/L-lactide composite for bone substitutes and scaffolds. In *Bioceramics*, vol. 18, (ed. T. Nakamura, K. Yamashita & M. Neo), pp. 1311–1314. Kyoto, Japan: Trans Tech Publications Ltd.

Hing, K. A., Best, S. M., Tanner, K. E., Bonfield, W. & Revell, P. A. 2004 Mediation of bone ingrowth in porous hydroxyapatite bone graft substitutes. *J. Biomed. Mater. Res. A* **68**, 187–200. (doi:10.1002/jbm.a.10050)

Ishaug-Riley, S. L., Crane, G. M., Gurlek, A., Miller, M. J., Yasko, A. W., Yaszemski, M. J. & Mikos, A. G. 1997 Ectopic bone formation by marrow stromal osteoblast transplantation using poly(DL-lactic-*co*-glycolic acid) foams implanted into the rat mesentery. *J. Biomed. Mater. Res.* **36**, 1–8. (doi:10.1002/(SICI)1097-4636(199707)36:1<1::AID-JBM1>3.0.CO;2-P)

Jarcho, M. 1981 Calcium phosphate ceramics as hard tissue prosthetics. *Clin. Orthop. Rel. Res.* **157**, 259–278.

Kasplan, F. S., Hayes, W. C., Keaveny, T. M., Boskey, A., Einhorn, T. A. & Iannotti, J. P. 1994 Form and function of bone. In *Orthopaedic basic science* (ed. S. R. Simon), pp. 127–184. Rosemont, IL: American Academy of Orthopaedic Surgeons.

Kawamura, M., Iwata, H., Sato, K. & Miura, T. 1987 Chondroosteogenetic response to crude bone matrix proteins bound to hydroxyapatite. *Clin. Orthop. Rel. Res.* **217**, 281–292.

Kondo, N., Ogose, A., Tokunaga, K., Ito, T., Arai, K., Kudo, N., Inoue, H., Irie, H. & Endo, N. 2005 Bone formation and resorption of highly purified beta-tricalcium phosphate in the rat femoral condyle. *Biomaterials* **26**, 5600–5608. (doi:10.1016/j.biomaterials.2005.02.026)

Kurashina, K., Kurita, H., Wu, Q., Ohtsuka, A. & Kobayashi, H. 2002 Ectopic osteogenesis with biphasic ceramics of hydroxyapatite and tricalcium phosphate in rabbit. *Biomaterials* **23**, 407–412. (doi:10.1016/S0142-9612(01)00119-3)

Lohmann, C. H., Tandy, E. M., Sylvia, V. L., Hell-Vocke, A. K., Cochran, D. L., Dean, D. D., Boyan, B. D. & Schwartz, Z. 2002 Response of normal female human osteoblasts (NHOst) to 17beta-estradiol is modulated by implant surface morphology. *J. Biomed. Mater. Res.* **62**, 204–213. (doi:10.1002/jbm.10290)

Lotz, J. C., Gerhart, T. N. & Hayes, W. C. 1990 Mechanical properties of trabecular bone from the proximal femur: a quantitative CT study. *J. Comput. Assist. Tomogr.* **14**, 107–114.

Mastrogiacomo, M., Scaglione, S., Martinetti, R., Dolcini, L., Beltrame, F., Cancedda, R. & Quarto, R. 2006 Role of scaffold internal structure on *in vivo* bone formation in macroporous calcium phosphate bioceramics. *Biomaterials* **27**, 3230–3237. (doi:10.1016/j.biomaterials.2006.01.031)

Montjovent, M. O., Mathieu, L., Hinz, B., Applegate, L. L., Bourban, P. E., Zambelli, P. Y., Manson, J. A. & Pioletti, D. P. 2005 Biocompatibility of bioresorbable poly(L-lactic acid) composite scaffolds obtained by supercritical gas foaming with human fetal bone cells. *Tissue Eng.* **11**, 1640–1649. (doi:10.1089/ten.2005.11.1640)

Mooney, D. J., Breuer, M. D., McNamara, K. M., Vacanti, J. P. & Langer, R. 1995 Fabricating tubular devices from polymers of lactic and glycolic acid for tissue engineering. *Tissue Eng.* **1**, 107–118.

Passuti, N., Daculsi, G., Rogez, J. M., Martin, S. & Bainvel, J. V. 1989 Macroporous calcium phosphate ceramic performance in human spine fusion. *Clin. Ortho. Rel. Res.* **248**, 169–176.

Quarles, L. D., Yohay, D. A., Lever, L. W., Caton, R. & Wenstrup, R. J. 1992 Distinct proliferative and differentiated stages of murine MC3T3-E1 cells in culture: an *in vitro* model of osteoblast development. *J. Bone Min. Res.* **7**, 683–692.

Rezwan, K., Chen, Q. Z., Blaker, J. J. & Boccaccini, A. R. 2006 Biodegradable and bioactive porous polymer/inorganic composite scaffolds for bone tissue engineering. *Biomaterials* **27**, 3413–3431. (doi:10.1016/j.biomaterials.2006.01.039)

Ripamonti, U. 1996 Osteoinduction in porous hydroxyapatite implanted in heterotopic sites of different animal models. *Biomaterials* **17**, 31–35. (doi:10.1016/0142-9612(96)80752-6)

Roy, T. D., Simon, J. L., Ricci, J. L., Rekow, E. D., Thompson, V. P. & Parsons, J. R. 2003 Performance of degradable composite bone repair products made via three-dimensional fabrication techniques. *J. Biomed. Mater. Res. A* **66**, 283–291. (doi:10.1002/jbm.a.10582)

Sasaoka, R., Terai, H., Toyoda, H., Imai, Y., Sugama, R. & Takaoka, K. 2004 A prostanoid receptor EP4 agonist enhances ectopic bone formation induced by recombinant human bone morphogenetic protein-2. *Biochem. Biophys. Res. Commun.* **318**, 704–709. (doi:10.1016/j.bbrc.2004.04.080)

Schindler, A. & Harper, D. 1979 Polylactide. II. Viscosity–molecular weight relationships and unperturbed chain dimensions. *J. Polym. Sci.* **17**, 2593–2599.

Shikinami, Y. 2003 Organic-inorganic compound porous body and manufacturing method thereof. JP Patent no. 159321.

Shikinami, Y. & Okuno, M. 1999 Bioresorbable devices made of forged composites of hydroxyapatite (HA) particles and poly-L-lactide (PLLA): part I. Basic characteristics. *Biomaterials* **20**, 859–877. (doi:10.1016/S0142-9612(98)00241-5)

Shikinami, Y., Matsusue, Y. & Nakamura, T. 2005 The complete process of bioresorption and bone replacement using devices made of forged composites of raw hydroxyapatite particles/poly L-lactide (F-u-HA/PLLA). *Biomaterials* **26**, 5542–5551. (doi:10.1016/j.biomaterials.2005.02.016)

Slivka, M. A., Leatherbury, N. C., Kieswetter, K. & Niederauer, G. G. 2001 Porous, resorbable, fiber-reinforced scaffolds tailored for articular cartilage repair. *Tissue Eng.* **7**, 767–780. (doi:10.1089/107632701753337717)

Tamai, N., Myoui, A., Tomita, T., Nakase, T., Tanaka, J., Ochi, T. & Yoshikawa, H. 2002 Novel hydroxyapatite ceramics with an interconnective porous structure exhibit superior osteoconduction *in vivo*. *J. Biomed. Mater. Res.* **59**, 110–117. (doi:10.1002/jbm.1222)

Vehof, J. W., Fisher, J. P., Dean, D., van der Waerden, J. P., Spauwen, P. H., Mikos, A. G. & Jansen, J. A. 2002 Bone formation in transforming growth factor beta-1-coated porous poly (propylene fumarate) scaffolds. *J. Biomed. Mater. Res.* **60**, 241–251. (doi:10.1002/jbm.10073)

Villanueva, A. R. & Mehr, L. A. 1977 Modifications of the Goldner and Gomori one-step trichrome stains for plastic-embedded thin sections of bone. *Am. J. Med. Technol.* **43**, 536–538.

Yang, S., Leong, K. F., Du, Z. & Chua, C. K. 2001 The design of scaffolds for use in tissue engineering. Part I. Traditional factors. *Tissue Eng.* **7**, 679–689. (doi:10.1089/107632701753337645)

Yuan, H., Zou, P., Yang, Z., Zhang, X., de Bruijn, J. D. & de Groot, K. 1998 Bone morphogenetic protein and ceramic-induced osteogenesis. *J. Mater. Sci. Mater. Med.* **9**, 717–721. (doi:10.1023/A:1008998817977)

Yuan, H., Kurashina, K., de Bruijn, J. D., Li, Y., de Groot, K. & Zhang, X. 1999 A preliminary study on osteoinduction of two kinds of calcium phosphate ceramics. *Biomaterials* **20**, 1799–1806. (doi:10.1016/S0142-9612(99)00075-7)

Wan, Y., Tu, C., Yang, J., Bei, J. & Wang, S. 2006 Influences of ammonia plasma treatment on modifying depth and degradation of poly(L-lactide) scaffolds. *Biomaterials* **27**, 2699–2704. (doi:10.1016/j.biomaterials.2005.12.007)